Revista Mexicana de Astronomía y Astrofísica, **00**, ??–?? (2007)

SPECTROSCOPIC ANALYSIS OF FOUR POST-AGB CANDIDATES

R. E. Molina,[1] S. Giridhar,[2] C. B. Pereira,[3] A. Arellano Ferro,[4,5] and S. Muneer[6]

Received ; accepted

RESUMEN

Hemos efectuado un análisis detallado de las abaundancias químicas de cuatro objetos candidatos a post-AGB; IRAS 13110 - 6629, IRAS 17579 - 3121, IRAS 18321 - 1401 y IRAS 18489 - 0629, usando espectros de alta resolución. Hemos construido las Distribuciones de Energía Espectral (SEDs) para cada objeto usando datos fotométricos existentes, combinados con los flujos infrarojos. Para todos los objetos en la muestra, las SEDs exhiben dos picos en la distribución de energía, con el pico IR bien definido, mostrando con ello la presencia de material circunestelar. Las abundancias de CNO muestran la producción de N por la vía del ciclo CN, mientras que el cociente [C/Fe] observado señala una mezcla de carbono producida por la combustión del He aunque el cociente C/O se mantiene menor que 1. Se observa un efecto moderado de separación gas-polvo en IRAS 18489 - 0629 y en IRAS 17579 - 3121 mientras que solo se observa una gran dispersión en la remoción selectiva en IRAS 18321 - 1401 y en IRAS 13110 - 6629, lo que indica que otros procesos afectan los patrones de abundancias observadas.

ABSTRACT

We have done a detailed abundance analysis of four unexplored candidate post-Asymptotic Giant Branch(AGB) stars IRAS 13110 - 6629, IRAS 17579 - 3121, IRAS 18321 - 1401 and IRAS 18489 - 0629 using high resolution spectra. We have constructed Spectral Energy Distributions (SED) for these objects using the existing photometric data combined with infrared (IR) fluxes. For all sample stars, the SEDs exhibit double peaked energy distribution with well separated IR peaks showing the presence of dusty circumstellar material. The CNO abundances indicate the production of N via CN cycling, but observed [C/Fe] indicates the mixing of carbon produced by He burning by third dredge up although C/O ratio remains less that 1. A moderate DG effect is clearly seen for IRAS 18489 - 0629 and IRAS 17579 - 3121 while a large scatter observed in depletion plots for IRAS 18321 - 1401 and IRAS 13110 - 6629 indicate the presence of other processes affecting the observed abundance pattern.

Key Words: FUNDAMENTAL PARAMETERS: ABUNDANCES; DEPLETION; STARS: POST-AGB STARS.

1. INTRODUCTION

Post-AGB (PAGB) stars, which represent the late stages of evolution of low and intermediate mass stars (0.8 – 8 $M_{\odot}$), are very important diagnostic tools to understand the evolutionary processes including AGB nucleosynthesis which is a major source of production of elements such as C, N, F, Al, Na and s-process elements. These products are dredged up to the surface due to mixing episodes thereby modifying the observed abundances of these stars. The synthesized elements are ejected into the Interstellar Medium (ISM) through strong mass-loss at the end of AGB evolution hence these stars significantly affect the chemical evolution of galaxies. In the super wind phase (at the end of AGB evolution), most of the outer stellar envelope is lost; consequently PAGB stars are surrounded by circumstellar envelopes and hence their spectral energy distribution generally exhibits two peaks. However, exceptional PAGBs without circumstellar envelopes have been detected.

The PAGB evolutionary model proposed by Iben and Renzini(1983) had been improvised by Groenewegen & de Jong (1993) and Boothroyd & Sackmann (1999) through better approximations for quantities like mass-loss and mixing length. More comprehensive models including detailed calculations of thermal pulses have been presented in Karakas, Lattanzio & Pole (2002), Herwig (2004) etc. A very comprehensive review of AGB evolutionary models for a full range of masses and metallicities can be found in Herwig (2005).

The canonical definition of PAGB stars as objects

[1]Laboratorio de Investigación en Física Aplicada y Computacional, Universidad Nacional Experimental del Táchira, CP 5001, Venezuela.

[2]Indian Institute of Astrophysics, Bangalore 560034, India

[3]Observatrio Nacional/MCTI, Rua Gen. Jos Cristino 77, Sao Cristovao, Rio de Janeiro, CEP 20921-400, Brazil

[4]Instituto de Astronomía, Universidad Nacional Autónoma de México, México.

[5]European Southern Observatory, Karl-Schwarzschild-Straβe 2, 85748, Garching bei München, Germany

[6]CREST Campus, Indian Institute of Astrophysics, Hosakote, India

showing strong enhancement of carbon (C/O > 1) and s-process elements is met by relatively smaller fraction of stars. Evolutionary models show that objects with a small range in masses (1.8 to 4.0 $M_{\odot}$) show carbon and s-process element enrichment while those with lower mass exhibit only the effect of CNO processing. More massive stars (M> 4.0 $M_{\odot}$) undergo Hot Bottom Burning (HBB) where carbon produced by He burning is converted to N, hence C/O remains < 1 but N is enhanced and transient production of Li is predicted.

The observational and theoretical developments made in the last two decades on PAGBs has been summarized in the excellent review by Van Winckel (2003) where the diverse chemical compositions observed for the central stars are compared with the predictions from evolutionary models. More recent developments based on extended sample of PAGBs, made using the extended wavelength coverage have augmented our understanding of PAGB classes including the morphology and chemistry of circumstellar shells as described in reviews by García-Lario (2006) and Giridhar (2011).

While the surface compositions of C-rich and O-rich PAGBs can be explained with AGB nucleosynthesis, mixing events and mass-loss; it has been noticed that chemical peculiarities not attributable to AGB nucleosynthesis are observed in a large fraction of PAGB stars including RV Tauri stars which show abundance patterns reflecting a systematic removal of condensable elements. Well known examples of such objects are HR4049, HD 52961, BD $+39^{o}4926$, HD 44179; a good summary could be found in Van Winckel (2003). The depletion of elements show strong correlation with condensation temperature T_C (defined as the temperature at which half of a particular element in a gaseous environment condenses into grains) ; those elements with higher T_C (easily condensable) are heavily depleted while those with lower T_C are largely unaffected. This removal of condensable elements onto the dust grain is commonly referred as dust-gas winnowing or DG-effect.

The full mechanism of DG effect is not yet fully understood, but it is generally believed to operate in a dusty circumbinary disks surrounding these objects as initially suggested by Waters, Trams & Waelkens (1992). From the study of SED of a large sample of PAGB stars De Ruyter et al. (2006) reported the presence of dust at or near sublimation temperature very close to the star for most depleted objects irrespective of their temperatures and ascribed it to the presence of gravitationally bound disk. With the help of high spatial resolution interferometry in mid IR, dusty disks around depleted objects Red Rectangle, HR 4049 and HD 52961 have been resolved (Deroo et al. 2007).

Sumangala Rao, Giridhar & Lambert (2012) have compiled the stellar parameters and abundances for PAGB stars and find that s-process enhanced group contains a very small number of binaries. However the depleted group contains larger fraction of binaries in accordance with the hypothesis of dusty disks surrounding binary post-AGB stars. Sumangala Rao & Giridhar (2014) have presented a similar compilation for RV Tauri stars. These authors also revisit the boundary conditions for discernible DG effect discussed in earlier papers by Giridhar et al. (2000, 2005). The values of minimum temperature and intrinsic metallicities are very similar for PAGB and RV Tauri stars.

The goal of this paper is to enlarge PAGB sample by a study of four candidate PAGB stars chosen from their location in the two color IRAS diagram. We have carried out detailed atmospheric abundance analysis using high resolution spectra for IRAS 13110 - 6629, IRAS 17579 - 3121, IRAS 18321 - 1401, IRAS 18489 - 0629, previously identified as post-AGB/PN objects (Preite-Martínez 1988; García-Lario et al. 1997; Pereira & Miranda 2007). We have also studied their spectral energy distribution to understand the properties of circumstellar material surrounding them.

The structure of the paper is as follows: § 2 presents the sample selection. We describe our observations and data analysis procedures in § 3. The estimation of atmospheric parameters, abundances and the errors associated with these parameters are presented, in § 4. The derived abundances for individual objects are reported. In § 5 these results are discussed. In § 6 and § 7 we present summary and conclusions.

2. THE SAMPLE

Fig. 1 shows the IRAS color-color diagram of van der Veen & Habing (1988) with different zones signifying the emergence and evolution of the circumstellar shell produced during AGB evolution. The objects in zone IV are undergoing super wind phase or slightly beyond; objects with only cold dust are found in V while VI b contains objects with warm and cold shells. Zone VIII and dashed area defined by García-Lario et al. (1997) is a region where, most post-AGB and planetary nebulae (PN) are found.

We have selected sample stars whose IR colors places them in zone VIII (IRAS 18321 - 1401) and the remaining three in the region where according to García-Lario et al. (1997) PAGB and PPN are found.

IRAS 13110 - 6629 (GLMP 342) was included in a sample of candidate PN objects by Silva et al. (1993) attempting to detect OH (1612 MHz, 1665 MHz and 1667 MHz) masers without success. Its position in the IRAS color-color diagram $[12]-[25]$ =+4.08 and $[25]-[60]=+0.30$, indicates that this object falls into the region defined by García-Lario et al. (1997) for PAGB stars and planetary nebulae. The presence of circumstellar material was detected by Clarke et al. (2005). This object has also been included in the Toruń catalog of Galactic PAGB (Szczerba et al. 2007; Szczerba et al. 2011) as a likely PAGB object.

The star IRAS 17579 - 3121 (GLMP 686) was classified as candidate PN by Preite-Martínez (1988) and Ratag et al. (1990) due to its infrared fluxes. Silva et al. (1993) reported the detection of a maser emission of OH at 1612 MHz (with double peaks) where they found velocities for the blue peak of 21 km s^{-1} and red peak 0 km s^{-1} respectively. Suárez et al. (2006) classified

this star as a PAGB star from its optical counterpart based on a low resolution spectrum. A more recent interferometric study using VLA by Gómez et al. (2008) did not confirm the association of IRAS 17579 - 3121 with the position of the radio continuum emission and conclude that this IRAS source is not likely to be a PN.

Given its position in the IRAS two color diagram IRAS 18321 - 1401 (PM 1-243) was classified as a possible PN by Preite-Martínez et al. (1988). This classification was questioned in a subsequent study by van de Steene & Pottasch (1995) who employed radio interferometric measurements to detect radio continuum emission at 6 cm which is characteristics of PN; but no emission was detected for this object. More recently, Pereira & Miranda (2007) classified the star as a PAGB star by comparing its spectrum with the spectrum of the known PAGB star GLMP 982. These authors suggest a spectral type F for this object.

The star IRAS 18489 - 0629 (PM 1-261) has been classified as a probable Planetary Nebula by Preite-Martínez (1988) following its location in the IRAS two color diagram. The large value of [12]-[25] = +3.05 color **might indicate** the presence of relatively warm dust resulting from a strong mass loss episode (Clarke et al. 2005). Pereira & Miranda (2007) from their study of 16 PAGB candidates using low resolution flux calibrated spectra have classified IRAS 18489 - 0629 as PAGB since the spectrum closely resembles that of GLMP 1058. By comparison with the spectrum of the supergiant star HD 9973, taken from the library of Jacoby et al. (1984), Pereira & Miranda (2007) suggested that the observed continuum energy distribution of IRAS 18489 - 0629 was similar to that of a reddened F5Iab star.

Basic information of the sample stars such as celestial and galactic coordinates, brightness, IRAS fluxes and its quality (in parenthesis) is given in Table 1. The apparent magnitudes V were obtained only for IRAS 18489 - 0629, IRAS 17579 - 3121 and IRAS 13110 - 6629 taken from different sources (Hog et al. 2000, SIMBAD[7] database and Perryman 1997).

2.1. *Photometric Variability*

Light variability in PAGB stars is of common occurrence. RV Tauris exhibit large amplitude light curve of distinct shape and periodicity but other PAGBs are known to exhibit small amplitude light variation as described by Kiss et al. (2007).

PAGB stars of intermediate temperature are found near or above the upper luminosity limit of the instability strip hence semi-regular pulsations are commonly seen. Their periodicities are not always firmly established and show irregular amplitude modulations and even cessation in their variability. Classical examples of variable PAGB stars are 89 Her (HR 6685), HD 161796 and LN Hya (HR 4912) with semi-periods of 63, 42-60 and 44-80 days (Arellano Ferro 1985; Arellano Ferro 1981).

[7]http://simbad.u-strasbg.fr/simbad/sim-fid

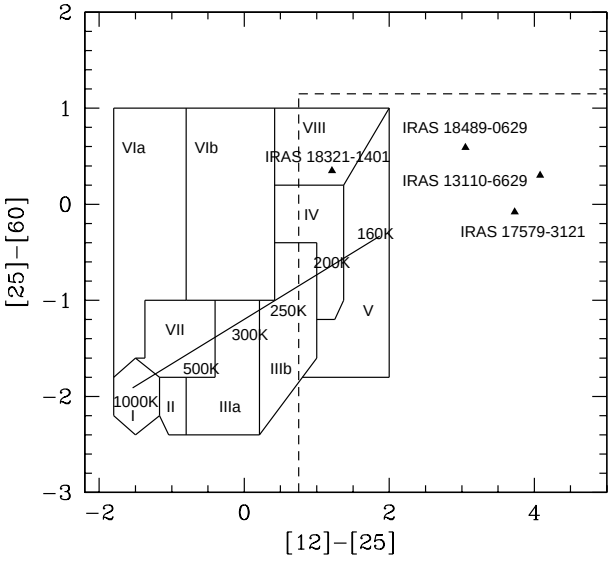

Fig. 1. The location of our sample stars in IRAS two color diagram is shown. The dotted-line represents the region limit by García-Lario et al. (1997). The regions represented with Roman numerals have been defined by van der Veen & Habing (1988).

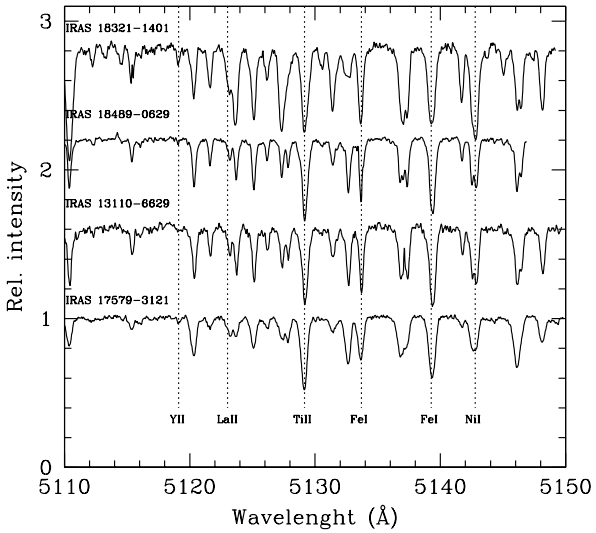

Fig. 2. Representative spectra of the sample stars IRAS 13110 - 6629 and IRAS 17579 - 3121. IRAS 18321 - 1401, IRAS 18489 - 0629, The location of lines of certain important elements have been indicated by dashed lines.

TABLE 1

BASIC DATA OF THE PROGRAM STARS. THE FLUX QUALITY IS GIVEN IN PARENTHESIS CODED FROM LOW TO HIGH AS FROM 1 TO 3 RESPECTIVELY.

No. IRAS	α_{2000} (h m s)	δ_{2000} (h m s)	V (mag)	l (^{0})	b (^{0})	F_{12} μm (Jy)	F_{25} μm (Jy)	F_{60} μm (Jy)	F_{100} μm (Jy)
13110 - 6629	13 14 27.4	−66 45 35.0	10.74	305.20	−3.98	0.55(3)	23.51(3)	30.91(3)	12.48(3)
17579 - 3121	18 01 13.3	−31 21 56.5	11.40	359.61	−4.13	2.01(3)	62.39(3)	58.21(3)	14.71(1)
18321 - 1401	18 34 57.2	−13 58 49.0	...	18.62	−2.75	0.36(1)	1.10(3)	1.52(3)	115.90(1)
18489 - 0629	18 51 39.1	−06 26 07.1	11.70	27.22	−2.97	0.27(1)	4.48(3)	7.49(3)	78.49(1)

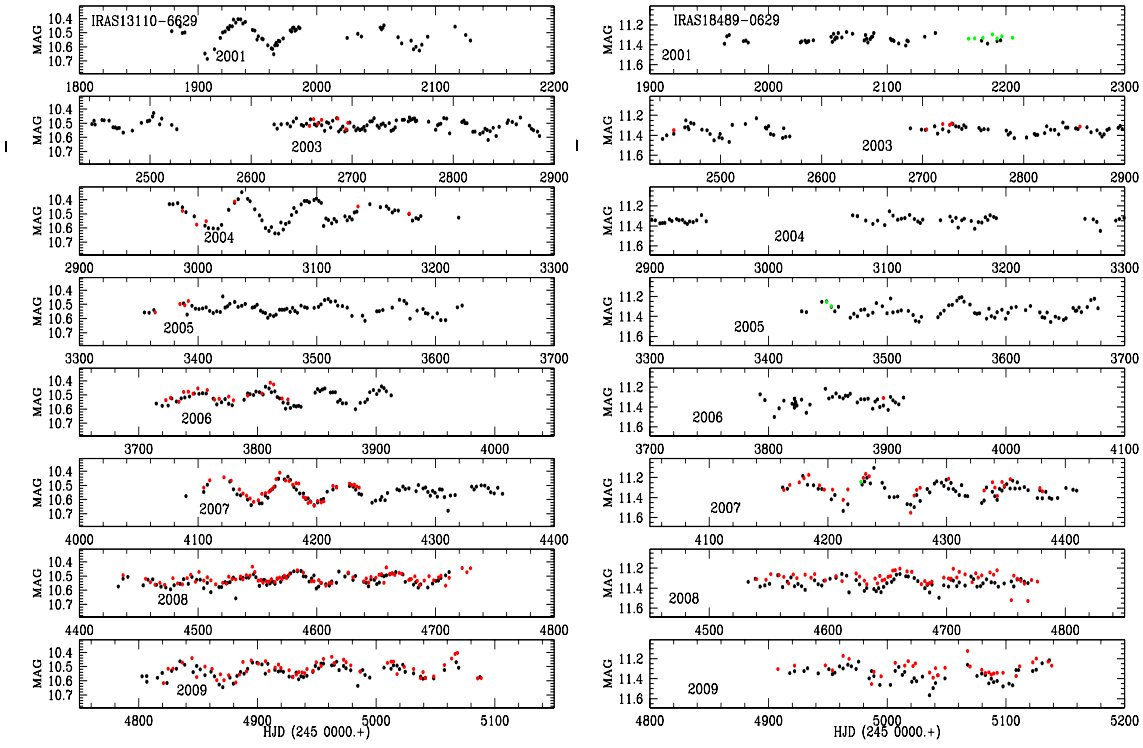

Fig. 3. Light variations in the stars IRAS13110−6629 and IRAS18489−0629 as seen from the V-band data from the All Sky Automated Survey. Each independent data set is depicted with a different Color. Year numbers are placed at the beginning of the calendar year for a reference. See § 2.1. for more details

Defining periodicities even using the radial velocity variations for PAGB is complicated since their radial velocities are often the combination of pulsations and differential motions in the extended atmosphere (Kloshkova & Panchuck 2012). On the other hand, dense and continuous photometry of PAGB stars is rare. In recent times the All Sky Automated Survey (ASAS) (Pojmanski 2002) provided valuable photometric data for a large number of objects. We have examined the V-band data obtained between 2001 and 2009 for all four stars in our sample. IRAS13110 - 6629 and IRAS18489 - 0629 display clear signs of variability of semi-regular nature, with amplitude modulations within 0.3 mag (Fig. 3). A frequency analysis of these data reveal characteristic times or semi-period between 52 and 58 d for IRAS13110 - 6629 and between 51.8 and 60.0 d for IRAS18489 - 0629. No secondary frequencies were identified. IRAS 17579 - 3121 and IRAS 18321 - 1401 do not show coherent variations but irregular fluctuations that range between 0.2 and 1.0 mag.

3. OBSERVATIONS AND REDUCTIONS

The high-resolution spectra of the stars analyzed in this work were obtained with FEROS, (Fiber-fed Extended Range Optical Spectrograph) at the 2.2 m ESO telescope at La Silla (Chile) on the nights of August 27, 2007 (IRAS 18489 - 0629), May 14, 2009 (IRAS 17579 - 3121), July 29, 2009 (IRAS 18321 - 1401) and July 31, 2009 (IRAS 13110 - 6629). For each star two exposure times of 3 600 secs were obtained. FEROS has a CCD with an array of 2048 × 4096 with each pixel size of 15μ, manufactured by EEV. The wavelength range obtained with FEROS covers the spectral region between 3900 and 9200Å and is distributed in 39 orders with a resolving power of $\lambda/\Delta\lambda = 48\,000$ or 2.2 pixels per $\Delta\lambda$, which gives, at 5000Å approximately 0.05Å/pixel (Kaufer et al. 1999).

The spectra were reduced following the standard procedure including bias subtraction, flat-fielding, order extraction and wavelength calibration with the MIDAS pipeline reduction package.

The cosmic ray hits causing narrow spikes were manually removed and all spectra were normalized to continuum. Two exposures were combined to get higher S/N ratios. The S/N ratio of the spectra was generally in the 120-150 range, however for the spectrum of IRAS 13110 - 6629 it was about 70 because one of the exposures was cut short due to cirrus. Since most of the sample stars are of intermediate temperatures, line blending was not severe. It was generally possible to measure line strengths with an accuracy of 5 to 8 percent.

Fig. 2 shows the representative spectra of the sample stars arranged in descending temperature sequence.

4. ATMOSPHERIC PARAMETERS

The spectral line strengths strongly depend on atmospheric parameters such as effective temperature $T_{\rm eff}$, gravity log g and microturbulence velocity ξ_t in addition to the abundances; hence a good determination of atmospheric parameters are mandatory to derive accurate abundances. The estimation of the effective temperature and gravity can be made from photometric and spectroscopic data.

4.1. *Photometric data*

Table 2 lists the magnitudes JHK for IRAS 13110 - 6629 and IRAS 17579 - 3121 IRAS 18489 - 0629, taken from the 2MASS photometry (Cutri et al. 2003). The color excess $E(B-V)$ was estimated from the reddening map of Schlegel et al. (1998). For $E(B-V) > 0.15$, we adopted the correction suggested by Bonifacio, Caffau & Molaro (2000). Then the intrinsic colors J_0, $(J-H)_0$ and $(H-K)_0$, were derived using the ratios $\frac{E(J-H)}{E(B-V)} = 0.322$ and $\frac{E(H-K)}{E(B-V)} = 0.183$ of Fiorucci & Munari (2003).

The effective temperatures for program stars were first derived using the $(J-H)_o$ calibrations for supergiant stars by Tokunaga (2000). These temperatures are given in Table 2 as $T_{\rm eff,Tok}$.

An independent estimates of temperatures, gravity and absolute magnitudes were made from intrinsic colors $(J-H)_o$ and $(H-K_s)_o$ calibrated by Molina (2012) for post-AGB and RV Tauri stars. They are presented as $T_{\rm eff_{Mol}}$, log g_{Mol} and M_J in Table 2. As shown in the figure 6 of Molina (2012), the calibration made using F-G supergiants gives systematically lower temperatures.

These photometric estimates of atmospheric parameters serve as starting values which are further refined by a detailed spectral analysis.

4.2. *Spectroscopic data*

We have used new grids of ATLAS9 model atmospheres available at the database of Kurucz (see Castelli and Kurucz 2003). We have used 2010 version of MOOG developed by C. Sneden (1973) in both line and spectrum synthesis mode. The assumptions made are local thermodynamic equilibrium (LTE), plane parallel atmosphere and hydrostatic equilibrium.

The atmospheric parameters $T_{\rm eff}$, log g and the microturbulence velocity ξ_t are obtained from the lines of well represented elements such as Fe, Ti and Cr.

The temperature was determined by requiring that there was no dependence of derived abundances on lower excitation using Fe I lines. Finally gravity was estimated from the ionization equilibrium of Fe I/Fe II, i.e. log n(Fe II)=log n(Fe I).

Attempts have been made to get a unique solution for temperature and gravity by studying the ionization equilibrium of several elements; Mg I & Mg II, Si I & Si II, Ti I & Ti II and Cr I & Cr II. The Balmer line profiles were affected by emission filling in hence we have explored the loci of Paschen lines in the temperature-gravity plane as it will be illustrated later in this paper (see Fig. 5).

The microturbulence ξ_t was estimated by requiring that the derived abundances are independent of the line strengths for a given specie. Generally, lines of

TABLE 2

2MASS PHOTOMETRY, INTRINSIC COLOR AND PHOTOMETRIC ATMOSPHERIC PARAMETERS FOR THE SAMPLE STARS.

No. IRAS	$J \pm \sigma_J$ (mag)	$H \pm \sigma_H$ (mag)	$K \pm \sigma_K$ (mag)	$E(B-V)_{IS}$ (mag)	$(J-H)_0$ (mag)	$(H-K)_0$ (mag)	J_0 (mag)	M_J (mag)	$T_{\rm eff,Tok}$ (K)	$T_{\rm eff,Mol}$ (K)	log g,Mol
13110 - 6629	8.06	7.60	7.40	0.50	0.30	0.15	7.62	−3.63±0.28	5864	6094±220	0.75±0.27
17579 - 3121	8.396±0.017	7.890±0.046	7.585±0.021	0.60	0.312	0.195	7.863	−3.48±0.28	5722	6023±220	0.78±0.27
18321 - 1401	...	...	...	...	...	...	...	...	...	...	...
18489 - 0629	9.006±0.027	8.63±0.05	8.398±0.029	0.51	0.213	0.139	8.560	−3.90±0.28	6733	6576±220	0.79±0.27

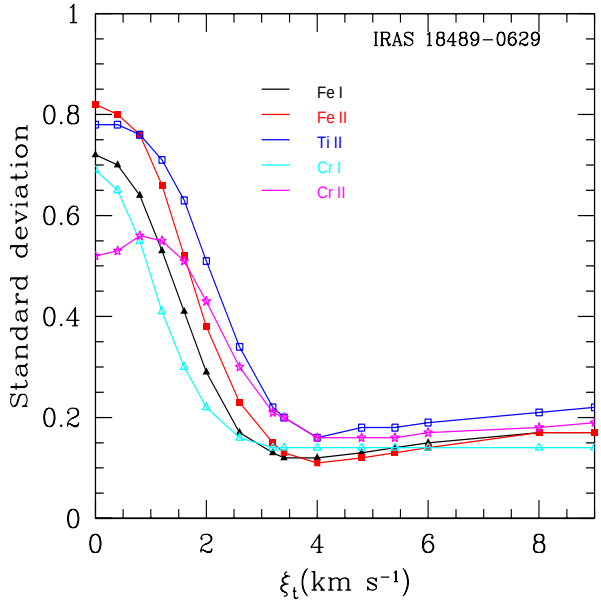

Fig. 4. Determination of microturbulence velocity for the star IRAS 18489 - 0629 using the plot of standard deviation as a function of microturbulence velocity ξ_t for several species in the 0 to 9 kms^{-1} range.

Fe II are preferred as it is known that they are not seriously affected by departure from LTE (Schiller & Przybilla 2008). For objects with very few measurable Fe II lines, Fe I lines were employed. In addition we have also employed the method described in Sahin & Lambert (2009) for estimating the microturbulence velocity based upon the measurement of standard deviation as a function of microturbulence velocity ξ_t for Fe I, Fe II, Ti II, Cr I and Cr II lines in the 0 to 9 km s^{-1} range. Fig. 4 illustrates the method using the star IRAS 18489 - 0629 as an example. The minimum standard deviation is reached for $\xi_t \sim 3.9$ km s^{-1}.

The measurement error in the equivalent widths (about 5 to 8 %), corresponds to uncertainty in microturbulence velocity of ± 0.2 km s^{-1} and in temperature and gravity of ± 200 K and ± 0.20 respectively. The adopted values of $T_{\rm eff}$, log g and ξ_t for our sample are listed in Table 3.

4.3. *Uncertainties in the elemental abundances*

The derived abundances are affected by errors in equivalent width measurements (which in turn depends upon the spectral resolution, S/N ratio, continuum placement and also on the spectral type of the star), errors in atomic data such as oscillator strengths (log gf) and errors in deriving the atmospheric parameters. The equivalent width measurement errors are random errors while errors caused by uncertainty in log gf and those in estimating atmospheric parameters are systematic errors. The effect of random errors in equivalent widths for a single star is well represented by σ_1, the standard deviation from the mean abundance based on the whole set of lines. These errors can be reduced by measuring a large number of lines.

The error in log gf values vary from element to element. For example, experimental values for Fe I and Fe II of high accuracy, better than 5 %, are available for a large fraction of lines. For other Fe-peak elements, errors in their gf values may range between 10 to 25%. For neutron-capture elements the accuracy of recent estimates are in 10% to 25% range. An extensive list of gf values for all important elements can be found in Sumangala Rao, Giridhar & Lambert (2012). The effect of systematic errors in abundances (in dex) caused by errors in estimating the atmospheric parameters are illustrated in Table 4 for two representative stars covering the temperature and gravity range of the sample stars. We present change in abundances caused by varying atmospheric parameters by 200 K, 0.20 and 0.2 km s^{-1} with respect to the chosen model for each star.

Following the standard procedure, the total systematic error σ_2 is estimated by taking the square root of the sum of the squares of each individual errors associated with uncertainties in temperature, gravity and microturbulence.

The total error σ_{tot} for each element is quadratic sum of σ_1 and σ_2. The error bars in abundance plot corresponds to this total error.

5. RESULTS FOR INDIVIDUAL STARS

The observed elemental abundances of the stars are governed by the composition of the natal ISM, the nucleosynthesis and mixing process in the course of its evolution and in some cases external effects such as mass exchange. For certain PAGBs and RV Tauri stars the DG effect introduces abundance anomalies.

The atmospheric abundances of all represented elements are given in Table 5 for the sample stars.

5.1. *IRAS 13110 - 6629*

For IRAS 13110 - 6629 (GLMP 342) the atmospheric parameters ξ_t, $T_{\rm eff}$ were derived from the study of a large number of Fe I and Fe II line; for the estimation of log g the ionization equilibrium between Fe I & Fe II as well as that of Mg I & Mg II, Ca I & Ca II, Ti I & Ti II, Cr I & Cr II were used. The spectroscopically derived values $T_{\rm eff}$ 6500K, log g 0.5 and ξ_t of 5.0 kms^{-1} as given in Table 3 are used for abundance

TABLE 3

ADOPTED ATMOSPHERIC PARAMETERS FOR THE PROGRAM STARS

No. IRAS	$T_{\rm eff}$ (K)	log g	ξ_t (km s^{-1})	$V_r(hel)$ (km s^{-1})	$V_r(LSR)$ (km s^{-1})	Date
13110−6629	6500	0.50	5.0	+11.5±0.5	+8.1	July 31, 2009
17579−3121	6500	0.00	4.7	+24.7±0.6	+34.3	May 14, 2009
18321−1401	5500	0.20	4.0	+32.7±0.6	+46.9	July 29, 2009
18489−0629	6500	0.50	3.9	+159.6±0.5	+175.3	August 27, 2007

TABLE 4

THE SENSITIVITY OF ABUNDANCES TO THE CHANGES IN THE MODEL ATMOSPHERIC PARAMETERS FOR TWO VALUES OF TEMPERATURE OF OUR SAMPLE STARS.

	IRAS 18489 - 0629 (6500 K)				IRAS 18321 - 1401 (5500 K)			
Species	Δ $T_{\rm eff}$ +200 K	Δ log g +0.20	Δ ξ_t +0.20	σ_{tot}	Δ $T_{\rm eff}$ +200 K	Δ log g +0.20	Δ ξ_t +0.20	σ_{tot}
C I	−0.07	−0.01	+0.02	0.07	−0.06	−0.12	−0.08	0.15
N I	−0.09	−0.06	+0.02	0.11	+0.07	−0.04	0.00	0.08
O I	+0.02	−0.04	+0.02	0.05	−0.02	−0.03	+0.01	0.03
Na I	−0.17	+0.05	+0.01	0.18	−0.05	+0.01	+0.01	0.05
Mg I	−0.22	+0.06	+0.01	0.23	−0.06	0.00	+0.02	0.06
Al I					−0.05	+0.01	+0.01	0.05
Si I	−0.17	+0.05	+0.01	0.18	−0.06	+0.01	+0.01	0.06
Si II	+0.08	−0.05	+0.02	0.10				
S I	−0.13	+0.01	+0.02	0.13	+0.01	−0.02	+0.01	0.02
Ca I	−0.24	+0.05	+0.02	0.25	−0.08	+0.01	+0.03	0.08
Sc II	−0.15	−0.05	+0.02	0.16	−0.04	−0.04	+0.03	0.06
Ti I	−0.27	+0.04	+0.01	0.27	−0.12	+0.01	+0.01	0.12
Ti II	−0.14	−0.06	+0.04	0.16	−0.04	−0.03	+0.03	0.05
V I					−0.12	+0.01	+0.01	0.12
V II	−0.13	−0.06	+0.04	0.15	−0.03	+0.03	+0.03	0.05
Cr I	−0.25	+0.04	+0.02	0.25	−0.09	+0.02	+0.03	0.09
Cr II	−0.07	−0.07	+0.05	0.11	−0.01	−0.04	+0.02	0.04
Mn I	−0.25	+0.04	+0.06	0.26	−0.09	−0.04	+0.01	0.09
Fe I	−0.21	+0.05	+0.03	0.22	−0.09	+0.01	+0.01	0.09
Fe II	−0.06	−0.05	+0.05	0.09	−0.05	−0.04	+0.04	0.07
Co I	−0.30	+0.04	0.00	0.30	−0.10	+0.01	+0.01	0.10
Ni I	−0.22	+0.04	+0.01	0.22	−0.08	+0.03	+0.01	0.08
Ni II	−0.07	−0.06	+0.01	0.09				
Cu I	−0.27	+0.04	+0.01	0.27	−0.12	+0.01	+0.02	0.12
Zn I	−0.22	+0.05	+0.02	0.23	−0.08	+0.01	+0.05	0.09
Y II	−0.16	−0.05	+0.02	0.17	−0.04	−0.03	+0.02	0.05
Zr II	−0.16	−0.06	+0.01	0.17	−0.04	−0.03	+0.01	0.05
Ba II	−0.30	+0.01	+0.03	0.30	−0.05	−0.02	+0.01	0.05
La II	−0.24	−0.03	−0.01	0.24	−0.05	−0.03	0.00	0.05
Ce II	−0.22	−0.04	0.00	0.22	−0.06	−0.03	+0.02	0.07
Nd II					−0.07	−0.03	+0.01	0.07
Eu II	−0.21	−0.03	+0.01	0.21	−0.06	−0.03	0.00	0.06

TABLE 5

ELEMENTAL ABUNDANCES FOR THE SAMPLE STARS.

		IRAS 13110 - 6629			IRAS 17579 - 3121			IRAS 18321 - 1401			IRAS 18489 - 0629		
Species	$\log \epsilon_{\odot}$	[X/H]	N	[X/Fe]	[X/H]	N	[X/Fe]	[X/H]	N	[X/Fe]	[X/H]	N	[X/Fe]
C I	8.39	−0.01±0.13	18	+0.27	+0.07±0.13	15	+0.39	−0.11±0.10	7	+0.32	−0.09±0.10	18	+0.27
N I	7.78	+0.47±0.14	5	+0.75	+0.60±0.07	5	+0.92	−0.19±0.16	3	+0.24	+0.01±0.07	5	+0.37
O I	8.66	+0.04±0.06	3	+0.32	+0.29±0.13	3	+0.61	+0.10±0.13	3	+0.53	−0.18±0.21	4	+0.18
Na I	6.17	−0.02±0.05	3	+0.26	+0.27±0.08	3	+0.59	−0.21±0.09	4	+0.22	−0.06±0.10	4	+0.30
Mg I	7.53	+0.09±0.15	4	+0.37	+0.03±0.09	1	+0.35	+0.07±0.10	3	+0.50	−0.13±0.14	3	+0.23
Mg II	7.53	+0.09±0.20	2	+0.37	+0.26±0.09	1	+0.58						
Al I	6.37							−0.66±0.06	2	−0.23			
Si I	7.51				+0.02±0.09	8	+0.34	−0.06±0.10	18	+0.37	−0.03±0.09	11	+0.33
Si II	7.51	−0.06±0.11	11	+0.22	+0.09±0.04	1	+0.41				−0.15±0.04	1	+0.21
S I	7.14	−0.04±0.05	syn	+0.24	+0.14±0.10	2	+0.46	−0.14±0.13	3	+0.29	+0.22±0.12	8	+0.58
Ca I	6.31	−0.35±0.13	16	−0.07	−0.52±0.09	9	−0.20	−0.62±0.11	8	−0.19	−0.52±0.08	16	−0.16
Ca II	6.31	−0.28±0.04	2	0.00	−0.44±0.04	1	−0.12						
Sc II	3.05	−0.69±0.17	6	−0.41	−0.87±0.12	5	−0.55	−0.70±0.15	7	−0.27	−1.06±0.12	5	−0.70
Ti I	4.90	−0.60±0.06	1	−0.32				−0.67±0.10	11	−0.24	−0.70±0.16	3	−0.34
Ti II	4.90	−0.52±0.10	7	−0.24	−0.72±0.10	8	−0.40	−0.66±0.13	8	−0.23	−0.59±0.13	12	−0.23
V I	4.00							−0.35±0.21	2	+0.08			
V II	4.00	−0.69±0.12	2	−0.41	−0.87±0.02	1	−0.55	−0.38±0.16	2	+0.05	−0.40±0.08	3	−0.04
Cr I	5.64	−0.37±0.13	8	−0.09	−0.54±0.10	4	−0.22	−0.54±0.15	12	−0.11	−0.48±0.17	9	−0.12
Cr II	5.64	−0.35±0.16	12	−0.07	−0.38±0.11	6	−0.06	−0.58±0.13	11	−0.15	−0.41±0.18	12	−0.05
Mn I	5.39	−0.40±0.17	5	−0.12	−0.40±0.14	4	−0.08	−0.74±0.12	7	−0.31	−0.55±0.12	5	−0.19
Fe I	7.45	−0.28±0.13	84		−0.34±0.14	73		−0.45±0.12	132		−0.33±0.12	55	
Fe II	7.45	−0.28±0.11	19		−0.29±0.09	17		−0.41±0.10	17		−0.39±0.12	9	
Co I	4.92	−0.45±0.08	1	−0.17				−0.31±0.14	4	+0.12	−0.33±0.08	1	+0.03
Ni I	6.23	−0.26±0.14	13	+0.02	−0.37±0.09	4	−0.05	−0.47±0.10	34	−0.04	−0.42±0.10	21	−0.06
Ni II	6.23	−0.20±0.12	2	+0.08	−0.39±0.04	1	−0.07				−0.44±0.04	2	−0.08
Cu I	4.21	−0.16±0.04	1	+0.12	−0.22±0.10	2	+0.10	−0.53±0.04	2	−0.10	−0.53±0.04	1	−0.17
Zn I	4.60	−0.37±0.07	3	−0.09	−0.36±0.08	2	−0.04	−0.25±0.14	4	+0.18	−0.35±0.10	3	+0.01
Y II	2.21	−0.96±0.05	3	−0.68	−1.33±0.06	4	−1.01	−1.28±0.10	5	−0.85	−1.41±0.16	4	−1.05
Zr II	2.59	−0.67±0.07	2	−0.39	−1.42±0.04	1	−1.10	−0.93±0.04	1	−0.50	−1.28±0.04	2	−0.92
Ba II	2.17	−0.40±0.07	1	−0.12	−0.85±0.07	1	−0.53	−1.55±0.07	1	−1.12	−0.84±0.07	1	−0.48
La II	1.13	−1.06±0.05	1	−0.78				−1.05±0.05	1	−0.62	−0.53±0.10	3	−0.17
Ce II	1.58				−1.48±0.09	1	−1.16	−0.99±0.16	4	−0.56	−1.02±0.15	2	−0.66
Nd II	1.45							−1.02±0.12	8	−0.59			
Sm II	1.01							−0.92±0.09	5	−0.49			
Eu II	0.52	−0.22±0.06	2	+0.06	−1.21±0.06	1	−0.89				−0.45±0.06	1	−0.09

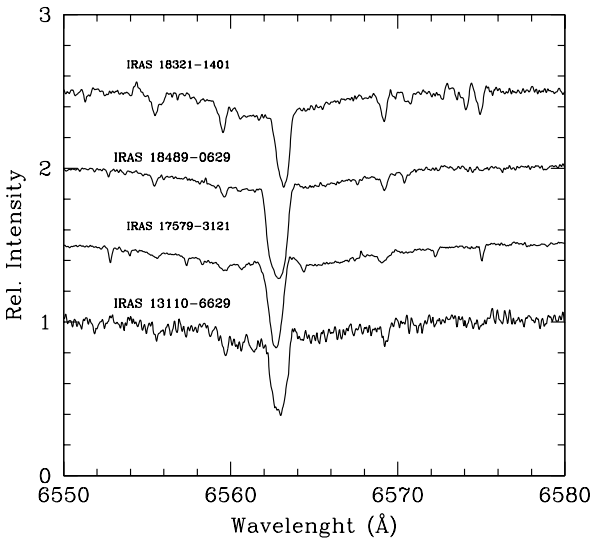

Fig. 6. Hα profiles in IRAS 18321 - 1401, IRAS 18489 - 0629, IRAS 17579 - 3121 and IRAS 13110 - 6629.

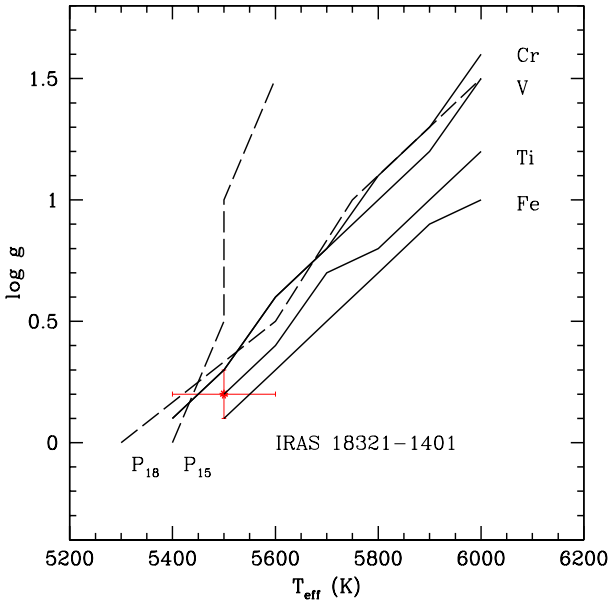

Fig. 7. The P15 (8545 Å) & P18 (8438 Å) and the ionization equilibrium loci for Fe, Cr, V, Ti are plotted in the temperature gravity plane for IRAS18321 - 1401. The red dot indicates the adopted values of $T_{\rm eff}$ and log g for the calculation of abundances.

analysis. The temperatures derived from photometry are systematically lower; errors in reddening correction for object surrounded by circumstellar material could be one of the possible reasons. The heliocentric radial velocity +11.5± 0.5 km s^{-1} on HJD 2455043.479 was derived using 167 lines.

This star also shows a marginal Fe deficiency with [Fe/H] = −0.28. Similar to IRAS 18489 - 0629, it exhibits a large number of C, N lines but [N/Fe] is a little larger, +0.75. Replenishment of C (used in CN processing) from triple α reactions is indicated by [C/Fe] of +0.27. The C/O ratio is ∼ 0.5. [α/Fe] as estimated from Mg, Si and S is +0.27 which together with small radial velocity does not make a very compelling case for thick disk population. Fig. 8 indicates a mild DG effect.

5.2. *IRAS 17579 - 3121*

For this star IRAS 17579 3121 (GLMP 686) we estimated $T_{\rm eff}$=5722K from the Tokunaga (2000) calibrations and $T_{\rm eff}$=6023 ± 220K, log g=0.78 ± 0.27 and M_J=−3.48 ± 0.28 mag from the Molina (2012). From excitation equilibrium of Fe I and Paschen line fit we estimated a temperature of 6500K and the ionization equilibrium of Fe I/Fe II, Ti I/Ti II, Cr I/Cr II led to the estimate of log g=0.0.

The photometric estimates of temperature are systematically smaller and log g larger. Although light variations are not yet reported for this object but variability in parameters observed for PAGBs could in addition to the errors in reddening estimate may possibly explain systematic differences in atmospheric parameters. The adopted parameters for IRAS 17579 - 3121 are $T_{\rm eff}$=6500K, log g=0.0 and ξ_t=4.7 km s^{-1} are used for deriving abundances.

The heliocentric radial velocity measured for the spectrum taken on HJD 2454966.844 using 86 lines is +24.7 ± 0.6 km s^{-1}.

The photospheric abundances of IRAS 17579 - 3121 shows a moderate metal-deficiency ([Fe/H]= −0.32). Among light elements, N shows significant enrichment [N/Fe] = +0.92 indicating strong signatures of CN cycle; while [C/Fe] of +0.39 points to the products of He burning being brought to the surface. We estimate [α/Fe] of +0.4 similar to thick disk value. We again find the signature of DG effect as illustrated in Fig. 8.

5.3. *IRAS 18321 - 1401*

There is no JHK photometry available for IRAS 18321 - 1401 to estimate the initial temperature. Hα and Hβ being affected by emission were not used as temperature indicators. However the matching of P15 (8545 Å) and P18 (8438 Å) profiles of Paschen lines with those synthesized for a set of model atmospheres covering a good range in temperature and gravities and the combination with the ionization equilibrium requirement for Fe, Cr, Ti and V led to a temperature value of ∼5500 K and surface gravity of log g=0.20. Fig. 7 shows the corresponding loci in the temperature-gravity plane.

From our spectrum obtained on HJD 2455042.632, we measure a heliocentric radial velocity of +32.7 ± 0.6 km s^{-1} using 141 clean lines.

The star is moderately metal-poor ([Fe/H]=−0.43). Like IRAS 13110 - 6629 and IRAS 18489 - 0629, IRAS 18321 - 1401 has a significant number of C I lines. Very mild enrichment of N and C is present. However this stars has smaller C/O ratio of ∼0.3. We find [α/Fe] of +0.38 similar to thick disk objects. This star also shows a moderate depletion of condensable elements similar to that observed in IRAS 18489 - 0629 (see Fig. 8). It should be noted that the scatter in the

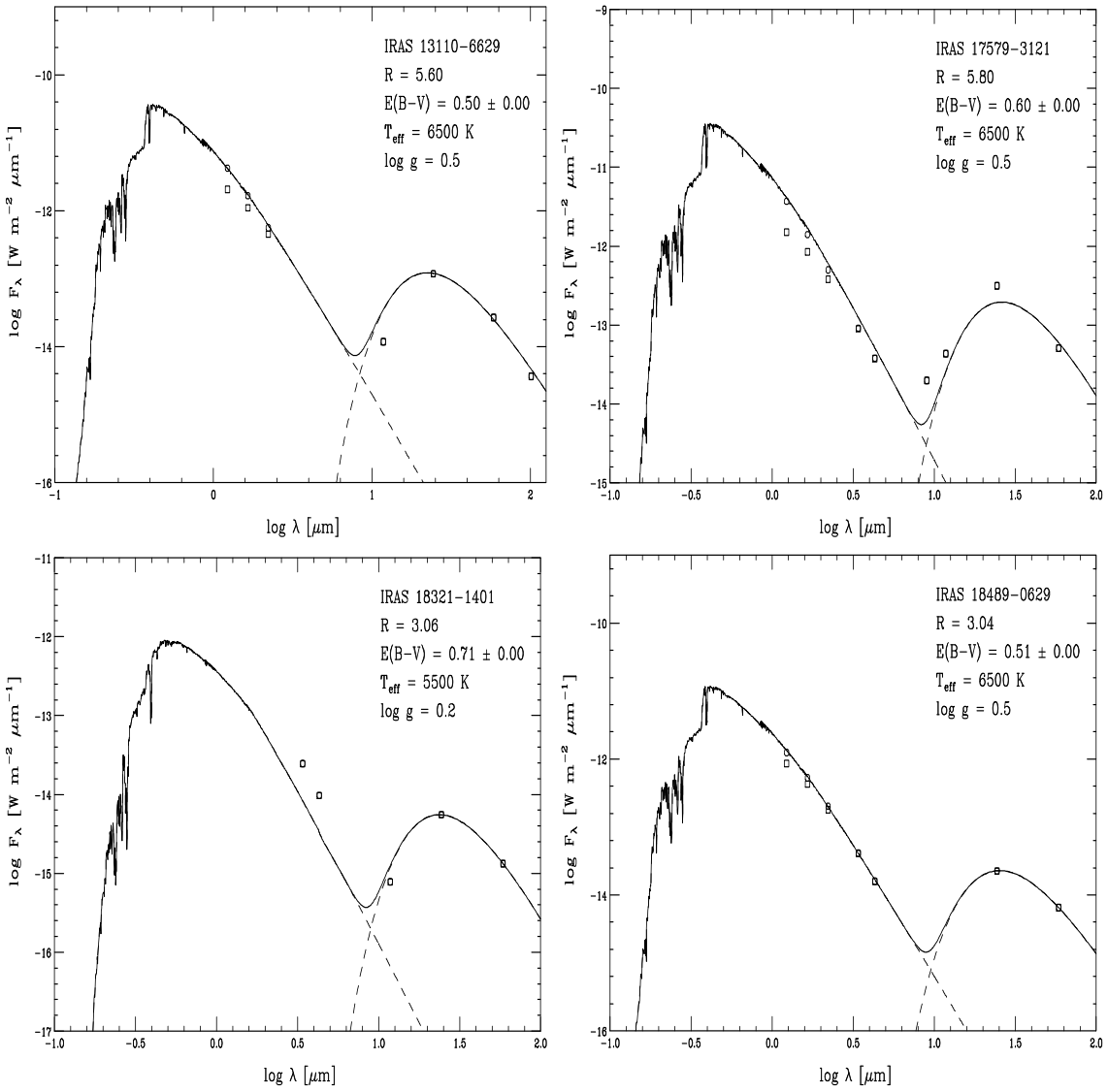

Fig. 5. The SED for the program stars is generated using the existing photometric data and IR colors as described in the text.

plot is much larger indicating the influence of other parameter/process.

5.4. *IRAS 18489 - 0629*

For IRAS 18489 - 0629 (PM 1-261) the estimated values of the atmospheric parameters based upon a large number of lines covering a large range equivalent widths, LEP and both stages of ionization used for the abundance analysis are listed in Table 3. The temperature estimated by spectroscopy is in good agreement with that indicated by the spectral type mentioned above as well as the photometric estimate given in Table 2.

From the spectrum taken on HJD 2454340.496 a heliocentric radial velocity of $+159.6 \pm 0.5$ km s^{-1} is measured using 223 clean unblended absorption lines that cover a wide spectral range. The present study is the first detailed abundance analysis made for this star using high resolution spectrum. The spectrum contained a large number of C and N lines. The star shows a mild iron deficiency ([Fe/H]= -0.36 ± 0.12). From Table 5 it can be seen that not only N shows small but significant enhancement indicating CN processing; C is replenished by the mixing of triple α products. We derive a C/O ratio of $\sim$ 0.8. IRAS 18489−0629 shows a mild Na-enrichment, [Na/Fe] = +0.30, probably caused by proton capture on ^{22}Ne. Although our study covers five α elements Mg, Si, S, Ti and Ca, we employ only Mg, Si and S to measure [α/Fe] since Ti and Ca are susceptible to non-LTE and are also affected by DG effect. The derived [α/Fe] of +0.38 together with large radial velocity makes it a likely thick disk object not withstanding a modest Fe deficiency. The Fe-peak elements V, Cr, Mn, Co, Ni vary in lockstep with Fe while s-process elements are significantly deficient. The abundance pattern can be easily understood via Fig. 8 which clearly shows the dependence of [X/H] on T_C. IRAS 18489−0629 belongs to the group of PAGBs showing systematic depletion of condensable elements.

6. DISCUSSION

In our study of unexplored PAGB candidates we find the signature of CN processing in all four sample stars although [N/Fe] ranges from +0.24 to +0.92. The measured [C/Fe] between +0.27 and +0.39 clearly shows the mixing of He burning products via the third dredge up (TDU). The sample stars have SEDs displaying a double peak (see Fig. 5) and the observed [α/Fe] in excess of +0.2 dex commonly seen in thick disk objects, which contain a large fraction of s-process enhanced PAGBs (see Table 9 of Sumangala Rao et al. 2012). However, none of the sample stars exhibit the expected enhancement of s-process elements. Instead, the observed [X/H] shows a dependence on T_C as demonstrated in (Fig. 8), although the extent of depletion varies over the sample. To quantify this effect, we could use the ratio of abundance of least affected elements like S and Zn (with low T_C), and the most affected ones such as Sc, Al and s-process elements. The potential candidates for the representation of intrinsic (unaffected) metallicity are S and Zn. But S being an α element, shows relative enrichment for the thick disk and halo stars. Zn on the other hand, remains unchanged over a large range in metallicities. Hence Zn is a better indicator of initial metallicity and has been used as reference to judge the relative enrichment of various elements. Among the elements most affected by the DG effect, Al and Zr are not well represented by many lines while Sc and Y measurements are based upon 4-5 lines. Hence we chose to define DG index as [Zn/H] - ([Sc/H]+[Y/H])/2.

In our sample, IRAS 18489 - 0629 with DG of 0.88 leads the group followed by IRAS 17579 - 3121 (0.74), IRAS 18321 - 1401 (0.67) and IRAS 13110 - 6629 (0.45) being the least depleted of the four. Another striking feature of the depletion pattern shown in Fig. 8 is the large scatter found for IRAS 18321 - 1401 and IRAS 13110 - 6629. The intriguing aspect of the sample is that three objects showing a range in DG index have the same $T_{\rm eff}$ of 6500K and not withstanding its lower temperature, IRAS 18321-1401 does not have lowest DG index. All four sample stars have temperatures larger than lower temperature limit required to sustain the depletion pattern against the mixing caused in the extended convective envelopes of cooler stars, which according to Sumangala Rao, Giridhar & Lambert (2012) is 4800K.

6.1. *The observed SEDs and Hα profile*

The SEDs for program stars were generated by comparing the archival photometric data with the theoretical SED fluxes given in Kurucz (1991) for models with atmospheric parameters given in Table 3 and adopting the interstellar extinction model by Steeman & The (1991). The ratio of total to selective extinction R= A_V/E(B-V) was estimated iteratively. We have used archival data from USNO, 2MASS, IRAS, AKARI, WISE and MSX6C available at NASA/IPAC Infrared Science Archive. We have omitted data with large errors e.g. IRAS with quality flag =1, 2MASS quality flag = E/X/U/F, MSX6C quality flag =1. The SEDs constructed for the program stars are shown in Fig. 5. A Planckian fit to the observed fluxes between 1.0 to 200μm leads to dust temperatures of 130K for IRAS 13110 - 6629, 110 K for IRAS 17579 - 3121, 120K for IRAS18324 - 1401 and 110K for IRAS 18489 - 0629. For IRAS 18321 - 1401 the scanty photometric data resulted in poor fit with the theoretically constructed SED.

Fig. 6 shows the profiles of Hα at 6562.8 Å of the program stars. All profiles have a broad shallow component and a deep narrow component with significant asymmetry. All profiles show indication of filling in by a rather central emission. Incipient P-Cygni structure is also seen in all cases. The P-cygni profiles (or inverse P-Cygni profiles) are of common occurrence in PAGB stars and are ascribed to the presence of a shock propagation in the pulsating atmospheres of these stars.

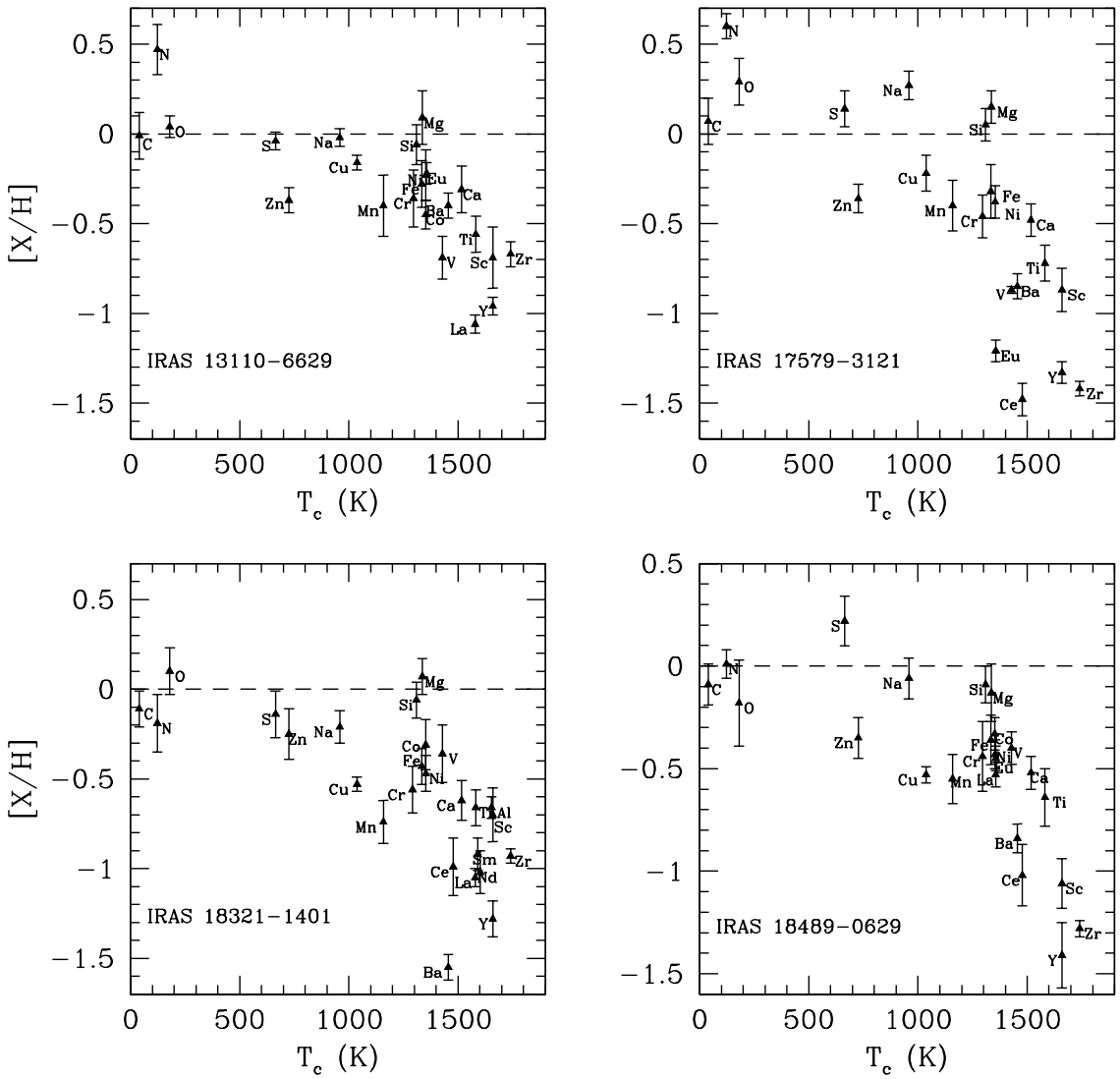

Fig. 8. Elemental abundances [X/H] as a function of condensation temperature T_c (Lodders 2003) for the sample stars.

6.2. *Overall abundance patterns*

We have observed a mild enrichment of [Na/Fe] $\sim$ +0.2 to +0.3 in IRAS 18489 - 0629, IRAS 13110 - 6629 and IRAS 18321 - 1401 and of +0.6 in IRAS 17579 - 3121. The enrichment of the latter object was measured from lines at 4979, 5682, 5688, 6160 Å, for which the non-LTE corrections do not exceed −0.10 dex (Gehren et al. 2004; Lind et al. 2011). This Na enhancement is probably due to a deep mixing that bring products of the Ne-Na cycle to the surface. The [α/Fe] measured using S, Si, Mg is similar to those found in thick disk objects although the observed metal deficiency is quite moderate. The observed [C/Fe] in the range +0.2 to +0.39 points to the mixing of He burning products being brought to the surface but accompanying s-process enhancement either did not take place or was obliterated by the depletion.

All four stars show depletion but a remarkable aspect of the abundance pattern is that only elements with T_C greater than 1300K are significantly affected. It is not clear if the observed depletion pattern is caused by insufficient mixing of depleted material with photospheric gas or temperature and compositional structure of circumstellar material favored condensation process only for high T_C elements.

To understand the large scatter present in the depletion diagram for IRAS18321 - 1401, we investigated the possible dependence of abundances on First Ionization Potentials (FIP) as suggested by Kameswara Rao & Reddy (2005). A plot of observed abundances as a function of FIP left panel of Fig. 9 clearly shows a reduced scatter. It appears that elements with FIP 8eV or lower show systematic depletion.

We also explored the possible dependence of observed abundance on the Second Ionization Potential (SIP) right column of Fig. 9 and do notice a significant depletion of elements with SIP lower than 13.6eV. It may be recalled that Luck & Bond (1989) had proposed that hydrogen Lyman continuum produced from a shock in the atmosphere over ionized elements with a SIP lower than 13.6eV, the Lyman limit. The Ca, Sc, and s-process elements Y, Zr, Ba, La, Ce, Sm Eu have lower SIP and hence could be over ionized relative to LTE estimate hence the LTE abundance analysis would yield systematically low abundance of these elements.

However, in the SIP plot the elements with similar SIP show different depletion. On the other hand, a smooth variation with FIP (with exception of Mg and Na) implies the systematic removal of species mostly present in first ionized state. The magnetically driven stellar wind proposed by García-Segura et al. (2005) for PAGB stars has the potential to remove the ionized species, but the presence of the stellar wind need to be established for this object. Although P-Cygni structure is mildly present in H_α the emission barely rises above continuum. Na D indeed exhibits a complex structure. This star deserves a multi-wavelength monitoring to understand the observed complex abundance pattern.

7. CONCLUSIONS

In this paper, we have performed a detailed atmospheric abundance analysis from high resolution spectra aimed to verify the evolutionary stage of a sample of four PAGB candidates IRAS13110 - 6629, IRAS 17579 - 3121, IRAS 18321 - 1401 and IRAS 18489 - 0629, selected from their infrared characteristics. None of them exhibit the s-process enhancement but clear indication of modest DG effect are observed for IRAS 18489 - 0629 and IRAS 17579 - 3121. For IRAS 13110 - 6629 and IRAS 18321 - 1401 the depletion diagram displays a large scatter. The scatter for IRAS 18321 - 1401 is significantly reduced in [X/H] vs FIP plot. Hence the possibility of outflowing magnetized column of gas systematically removing the singly ionized specie need to be explored. Another competing scenario is proposed by Luck & Bond (1989) wherein the Lyman α photons from a shock in the atmosphere over ionized elements with SIP less than the Lyman limit, 13.6eV. While SIP plot displays a larger scatter than FIP; the later requires magnetic field driven wind which are not easy to explain. In either case a systematic time series spectral monitoring to detect the events of strong shocks and possible manifestation of stellar wind is required.

The long-term photometric monitoring from the All Sky Automated Survey (ASAS) shows that IRAS13110 - 6629 and IRAS18489 - 0629 display periodic variations with characteristic times between 52 and 60 days, with amplitudes in the 0.2-0.3 magnitude range. The origin of these variations is most likely pulsational and are of a very similar nature to those in other well known PAGB of intermediate temperature, such as 89 Her, HD 161796 and LN Hya. IRAS 17579 - 3121, IRAS 18321 - 1401 display fluctuations of a few hundredths of magnitudes but no periodicities were found. Multi-wavelength observations are required for better understanding of these objects.

Acknowledgments

AAF acknowledges the support of DGAPA-UNAM grant through project IN104612. This work has made extensive use of SIMBAD database, 2MASS (Two Micron All Sky Survey, which is a joint project of the University of Massachusetts and the Infrared Processing and Analysis Center/California Institute of Technology, funded by the National Aeronautics and Space Administration and the National Science Foundation), IRAS, AKARI/IRC data (a JAXA project with participation of ESA), WISE(Wide-field Infrared Survey Explorer, which is a joint project of the University of California, Los Angeles, and the Jet Propulsion Laboratory/California Institute of Technology, funded by the National Aeronautics and Space Administration), MSX6C(Midcourse Space Experiment funded by the Ballistic Missile Defense Organization with additional support from NASA Office of Space Science) and the ADS-NASA to which we are thankful. We would also like to express our gratitude to anonymous referee for his/her comments which have helped in improving the paper considerably.

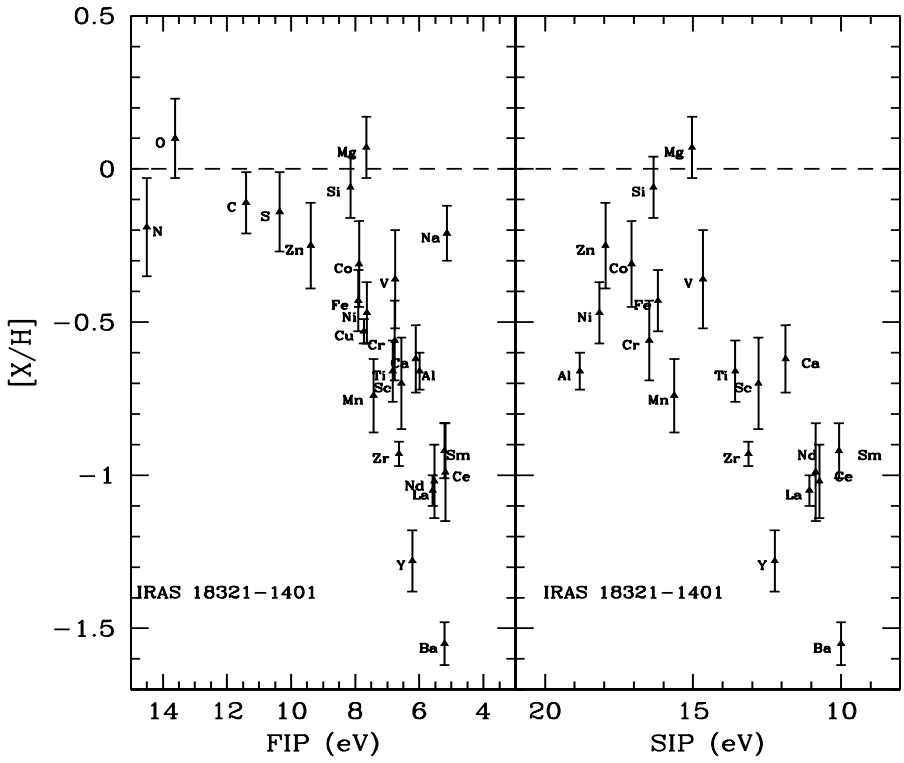

Fig. 9. Abundances [X/H] versus FIP and SIP for IRAS18321 - 1401.

REFERENCES

Arellano Ferro, A., 1985, RMA&A, 11, 113

Arellano Ferro, A., 1981, PASP, 93, 351

Bonifacio, P., Caffau, E., Molaro, P., 2000, A&AS, 145, 473

Boothroyd, A.I., Sackmann, I.J., 1999, ApJ, 510, 232

Castelli, F., Kurucz, R.L., 2003, in Piskunov N., Weiss W.W., Gray D.F., eds, Proc. IAU Symp. 210, Modelling of Stellar Atmospheres. Astron. Soc. Pac., San Fransisco, p. A20

Clarke, A.J., Oudmaijer, R.D., Lumsden, S.L., 2005, MNRAS, 363, 1111

Cutri, R.M., et al., 2003, VizieR On-Line Data Catalog: II/246

Deroo, P., Acke, B., Verhoelst, T., Dominik, C, Tatulli, E., Van Winckel, H., 2007, A&A, 474, 45

De Ruyter, S., Van Winckel, H., Maas, T., Lloyd Evans, T., Waters, L.B.F.M., Dejonghe, H., 2006, A&A, 448, 641

Fiorucci, M, Munari, U., 2003, A&A, 401, 781

García-Lario, P., Manchado, P., Pych, W., Pottasch, S.R., 1997, A&AS, 126, 479

García-Lario, P, . 2006, in Planetary Nebulae in our Galaxy and Beyond, Proceedings of the International Astronomical Union, Symposium #234. Edited by Michael J. Barlow and Roberto H. Méndez. Cambridge: Cambridge University Press, 2006., pp.63-70

García-Segura, G., López J.A., Franco, J., 2005, ApJ, 618, 919

Gehren, T., Liang, Y.C., Shi, J.R., Zhang, H.W., Zhao, G., 2004, A&A, 413, 1045

Giridhar, S. 2011, ASInC, 3, 39

Giridhar, S., Lambert, D.L., González, G., 2000, ApJ, 531, 521

Giridhar, S., Lambert, D. L., Reddy, B. E., Gonzalez, G., Yong, D., 2005, ApJ, 627, 432

Gómez, J.F., Suárez, O., Gómez, Y., Miranda, L.F., Torrelles, J.M., Anglada, G., Morata, O., 2008, AJ, 135, 2074

Gronewegen, M.A.T., de Jong, T., 1993, A&A, 267, 410

Herwig, F. 2004, ApJS, 155, 651

Herwig, F. 2005, ARA&A, 43, 435

Hog, E., Fabricius, C., Makarov, V.V., et al. 2000, A&A, 355, L27-30

Iben, I., Renzini, A., 1983, ARA&A, 21, 271

Jacoby, G.H., Hunter, D.A., Christian, C.A., 1984, ApJS, 56, 257

Kameswara Rao, N., Reddy, B.E., 2005, MNRAS, 357, 235

Karakas, A.I., Lattanzio, J.C., Pols, O.R., 2002, PASA,19, 515

Kaufer, A., et al., 1999, The Messenger, 95, 8

Kiss L.L., Derekas A., Szabó, Gy. M., Bedding T.R., Szabados L., 2007, MNRAS, 375, 1338

Klochkova, V.G., Panchuk, V.E., 2012, ARep., 56, 104

Kurucz, R. L. 1991, Precision Photometry: Astrophysics of the Galaxy, 27

Lind, K., Asplund, M., Barklem, P.S., Belyaev, A.K., 2011, A&A, 528, 103

Lodders, K. 2003, ApJ, 591, 1220

Luck, R.E., Bond, H.E., 1989, ApJ, 342, 476

Molina, R.E. 2012, RMA&A, 48, 95

Pereira, C.B., Miranda, L.F. 2007, A&A, 462, 231

Perryman, M.A.C., 1997, ESA - SP 1200, 0

Pojmanski, G. 2002, Acta Astronomica, 52,397

Preite-Martínez, A., 1988, A&AS, 76, 317

Ratag, M.A., Pottasch, S.R., Zijlstra, A.A., Menzies, J, 1990, A&A, 233, 181

Steenman, H., The, P. S. 1991, Ap&SS, 184, 9

Sahin, T., Lambert, D.L., 2009, MNRAS, 398, 1730

Silva, A.M., Azcarate, I.N., Poppel, W.G.L., Likkel, L., 1993, A&A, 275, 510

Schiller, F., Przybilla, N., 2008, A&A, 479, 849

Slysh, V.I., Dzura, A.M., Val'tts, I.E., & Gerard, E., 1997, A&AS, 124, 85

Schlegel, D.J., Finkbeiner, D.P., Davis, M., 1998, ApJ, 500, 525
Sneden, C., 1973, PhD Thesis, Univ. of Texas, Austin
Suárez, O., García-Lario, P., Manchado, A., Manteiga, M., Ulla, A., Pottasch, S.R., 2006, A&A, 458, 173
Sumangala Rao, S., Giridhar, S., Lambert, D.L. 2012, MNRAS, 419, 1254
Sumangala Rao, S., Giridhar, S., 2013, RMAA, 50, 49
Szczerba, R., Siodmiak, N., Stasinska, G., Borkowski, J., 2007, A&A, 469, 799
Szczerba, R., Siodmiak, N., Stasinska, G., Borkowski, J., 2011, ASP Conf. Ser., 445, 175
Tokunaga A. T., 2000, in Allen's Astrophysical Quantities, 4th edition, ed. A.N. Cox, Springer-Verlag (New York), p. 143
Van de Steene, G.C. & Pottasch, S.R., 1995, A&A, 299, 238
Van der Veen, W.E.C.J., Habing, H.J., 1988, A&A, 194, 125
Van Winckel, H., Waelkens, C., & Waters, L.B.F.M., 1995, A&A, 293, L25
Van Winckel, H., Waelkens, C., Fernie, J. D., & Waters, L. B. F. M. 1999, A&A, 343, 202
Van Winckel, H., 2003, ARA&A, 41, 391
Van Winckel, H., Lloyd Evans, T., Briquet, M.,; De Cat, P., Degroote, P., De Meester, W., De Ridder, J., Deroo, P., Desmet, M., Drummond, R., and 21 coauthors 2009, A&A, 505, 1221
Waters, L.B.F.M., Trams, N.R., Waelkens, C., 1992, A&A, 262, L37

R. E. Molina: Laboratorio de Investigación en Física Aplicada y Computacional, Universidad Nacional Experimental del Táchira, Venezuela, (rmolina@unet.edu.ve).
S. Giridhar: Indian Institute of Astrophysics, Bangalore 560034, India (giridhar@iiap.res.in).
C. B. Pereira: Observatrio Nacional/MCTI, Rua Gen. Jos Cristino 77, Sao Cristovao, Rio de Janeiro, CEP 20921-400, Brazil (claudio@on.br).
A. Arellano Ferro: Instituto de Astronomía, UNAM, Apartado Postal 70-264, 04510, México, D. F., México (armando@astro.unam.mx).
S. Muneer: CREST Campus, Indian Institute of Astrophysics, Hosakote, India (muneers@iiap.res.in).